1. Introduction

Imaging on a micro to nanometer scale is essential for many fields of modern science and technology. Besides the tremendous advances in electron, optical and scanning probe microscopy techniques in the last four decades, X-ray counterparts have been developed using highly brilliant synchrotron radiation. Over the last 15 years, in particular, these methods have bloomed following the proliferation of 3rd generation synchrotrons using undulator sources.

There are many benefits to using X-ray radiation, in particular soft X-rays in the energy range of 200 to 2000 eV, for microscopy. With wavelengths from 0.5 to 5 nm, the potential increase in resolution compared to optical light is obvious, even if constraints in optics currently reduce this to 10 nanometer at best in practice.

The main advantage is the way X-rays interact with matter; soft X-rays can penetrate, depending on energy and material, several hundred nanometer into and through a sample. This presents an excellent trade-off of penetration power and contrast. It allows the study of materials with multiple, hidden layers and the observation of heterogeneous particles while still having enough contrast to resolve small features of low optical depth.

This is emphasised by the contrast mechanisms available to X-ray microscopy. By selecting the photon energy to resonantly excite core electrons of a target material into unoccupied density of space, it is possible to directly and quantitatively observe not only the local distribution of elements, but also their chemical environment. Together with the high optical densities when resonantly exciting, this allows quantitative mapping of materials and even full spectroscopy without sacrificing spatial resolution.

For magnetic materials in particular, the X-ray magnetic circular dichroism (XMCD) effect provides an extremely strong magnetic contrast at L and M edges, especially for the relevant 3d and 4f elements. This allows direct, element specific imaging of magnetization inside the observed material with high contrast. Together with the ability of spectro-microscopy, this also allows the mapping magnetic moments of materials with the full resolution of the X-ray microscope.

For dynamic phenomena, the fact that X-ray light for microscopy is generated by synchrotrons becomes important. The light is emitted in stroboscopic short and regular flashes. This provides the use of pump-and-probe tech-

niques to resolve magnetization dynamics down to timescales below 50 ps while retaining all other advantages.

All of these abilities make X-ray microscopy the ideal method to study magnetization dynamics, on both sub-micrometer length and sub-nanosecond time scale with high fidelity and throughput.

In terms of spatial resolution, this allows access to the fundamental length scales of exchange length, domain pattern, domain wall width or grain sizes in magnetic structures.

The temporal resolution is also well matched to the timescales of fundamental processes like domain wall motion, precessional motion and spin-wave velocities.

Thus, the experimental access to this value is of great importance for the basic exploration and understanding of magnetic phenomena. On the other hand, from the technological aspect, the magnetization characteristics and their time evolution is essential for the realization of advanced spintronic devices and their applications as fast nano- to microscale sensors, storage media or logical devices.

Magnetic structures in the nanometer range are normally single domain particles. For sizes larger than 100 nm and wide aspect ratios in certain soft magnetic materials, a vortex state — respectively a Landau state, depending on whether the particle is circular or square — can be the preferred configuration. In those, the magnetization forms a loop, either steady in a single domain (the vortex state) or in four domains with 90 degree magnetization direction change between them (the Landau configuration). In the center of either, an only $\approx 20\,\mathrm{nm}$ wide vortex core is situated, in which the spins are forced out of plane due to exchange interaction.

The first direct imaging of these vortex cores after the turn of the century caused a strong increase in interest in these structures, in particular after direct investigation verified their minuscule size.

In 2006, shortly before the start of this thesis, it was discovered that the vortex core polarity can be dynamically switched with continuous microwave excitation with fields as low as single mT. This pushed such structures again to the forefront of research interest, as in contrast to the previously required static switching fields of 100s of mT, the new method of switching opened the door to using vortex core in complex devices.

The scope of this work was twofold:

Firstly, the aim was to extend the research in vortex core polarity switching, focusing on reversal by short pulses and the exploration of this switching scheme by micromagnetic simulations and direct imaging of the processes by magnetic scanning X-ray microscopy. These experiments were conducted at

the Canadian Light Source in Saskatoon and the Advanced Light Source in Berkeley, the place of previous efforts of the group.

Positive experiences with the techniques resulted in plans of the MPI-MF (since 2011, MPI-IS) to locally build its own scanning X-ray microscope, to establish local competence and capability in magnetic spectromicroscopy.

The second part of this thesis concerned the realization and commissioning of a new advanced scanning X-ray microscopy (called MAXYMUS - Magnetic X-ray Microscope and UHV Spectrometer) at the BESSY II synchrotron operated by the Helmholtz Zentrum Berlin.

This included work on speed and stability of the sample positioning using both sample as well as zone plate scanning, improving the vacuum system to achieve true UHV capability and optimizing the beamline to provide optimal illumination conditions in terms of coherence, flux and stability.

Special focus, however, was centered on the realization of very fast dynamic data acquisition setup, including work on optimizing single photon detection to provide unique possibilities of dynamic studies.

Part I.

Scanning X-Ray Microscopy: Basics and Background

2. Synchrotron Radiation

2.1. Creation and Properties of Synchrotron Radiation

2.1.1. Background: Bending Magnet Radiation

The original way of producing X-rays in synchrotron facilities was a side-effect of its operation principle; by using magnets to guide electrons on a circular path, they are accelerated and thus emit electromagnetic radiation.

This so-called Bending Magnet Radiation is characterized by a broad distribution of wavelengths in the range from the infrared and optical region (where it was first observed in 1947 [1]) up to the hard X-ray range for modern synchrotron facilities with high electron energies.

The spectrum itself is defined by a characteristic energy E_c as the central energy of the spectrum, in that half of the emitted energy is above, half below this value [2]:

$$E_c = \hbar\omega_c = \frac{3e\hbar B\gamma^2}{2m} \tag{2.1}$$

with B being the magnetic field of the bending magnet, m the mass of the electron at rest, e the elemental charge of the electron and γ the Lorentz factor

$$\gamma = \frac{1}{\sqrt{1-\frac{v^2}{c^2}}} \tag{2.2}$$

with v being the velocity of the electrons and c being the speed of light. The radiation itself is emitted into a narrow beam tangential to the electron trajectory with an opening angle of about γ^{-1} radians.

The amount of emitted radiation also directly scales with the number of electrons passing the bending magnet, i.e. the *current* in the synchrotron. An example of such a spectrum for BESSY II is shown in Fig. 2.1.

2.1.2. Radiation Creation Using Undulators

In order to create more intense X-ray radiation than possible with bending magnets so-called undulators can be used. In an undulator a periodic assembly of magnets with a period λ_U creates a field which forces electrons on undulating paths as shown in Fig. 2.2.

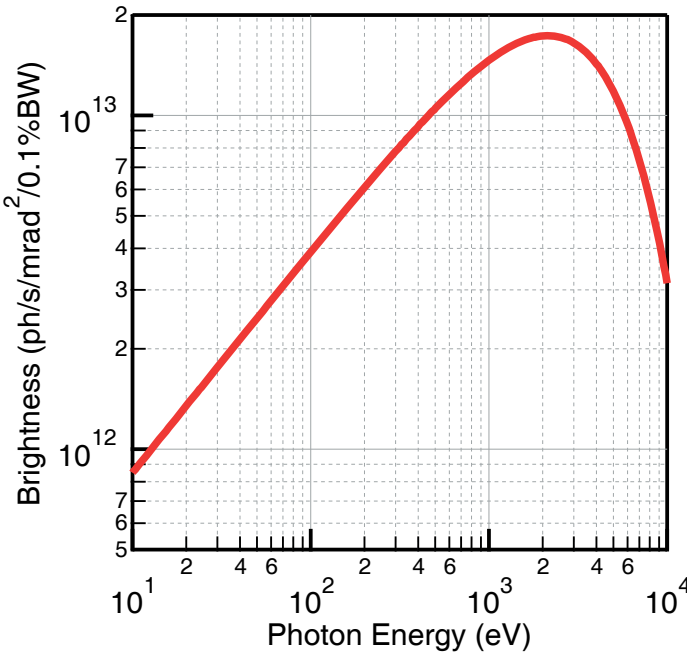

Figure 2.1: On-axis emission spectrum of a bending magnet at BESSY II. Parameters are 300 mA ring current, 1.72 GeV electron energy and 1.33 T bending magnet field strength [3].

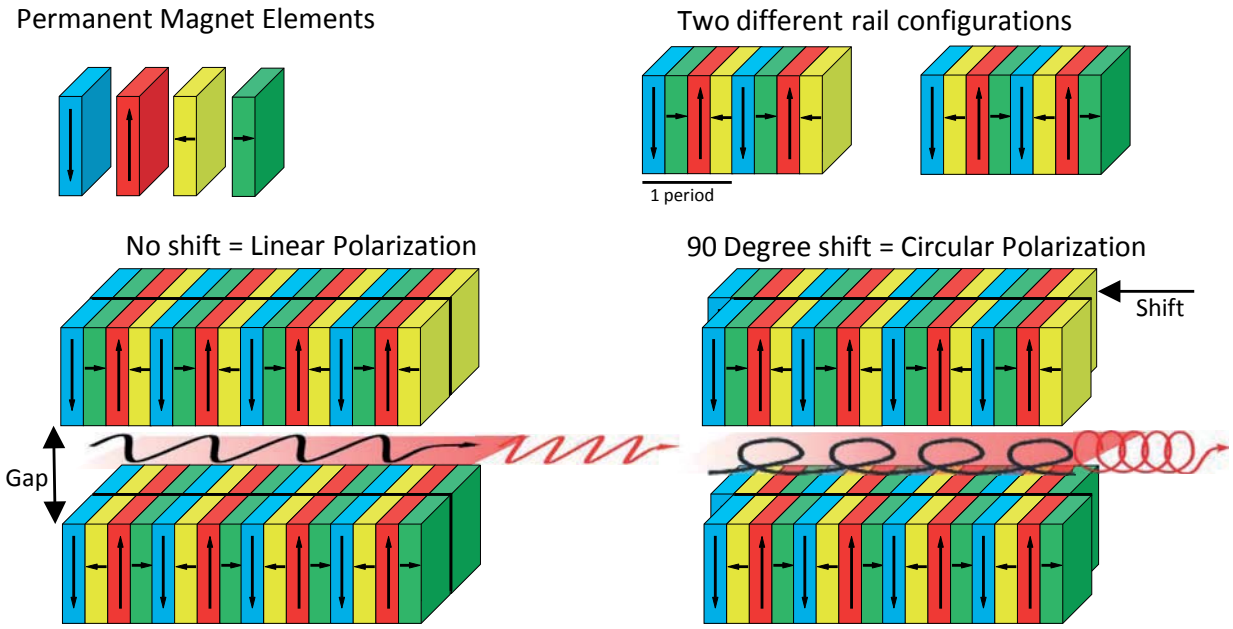

Figure 2.2.: Operation principle of an APPLE type undulator. The main components are rails made out of permanent magnets with adjustable gap. The magnetic field generated by them forces the electron beam into an undulating motion, emitting horizontally polarized light. APPLE type undulators have both top and bottom rails split into two, with the ability to shift them with regards to each other. This forces the electron beam into a helical motion (as shown on the right), emitting circular polarized x-rays.

An oscillating electron will emit electromagnetic radiation. But to understand the emission of photons as energetic as X-rays from periods in the centimeter range, the relativistic motion of the electrons has to be considered: The speed of electrons in synchrotrons is very close to the speed of light, with values for γ of over 1000 (approx. 3360 in case of BESSY II).

A rough way to understand the emission pattern and spectrum is shown in Fig. 2.3. In the reference frame of the average electron motion the undulator approaches the stationary electron with a speed close to c. This relativistic motion compresses its period:

$$\lambda'_U = \frac{\lambda_U}{\gamma} \tag{2.3}$$

In its reference frame the electron will oscillate according to the higher frequency of field change it observes due to the compressed undulator period, acting as a dipole emitter radiating electromagnetic waves with a wavelength of λ_U.

This radiation is emitted in the frame of reference of the electron and appears blue-shifted in the laboratory frame of reference. On axis, this yields a final wavelength proportional to λ_U/γ^2. Modern synchrotron sources have undulator periods in the cm range and create X-rays with wavelengths down to the sub-nanometer range.

A comparison of the output intensity of undulators with other sources of X-ray radiation can be seen in Fig. 2.4.

Polarity When using a linear undulator, as shown on the left in Fig. 2.2, the electrons oscillate in a plane, creating linear polarized light with a polarization direction parallel to the ground (horizontal polarization). By splitting both rails along the length of the undulator and shifting them relative to each other (shown on the right side of Fig. 2.2), the creation of both circular polarized light by forcing the electrons on a helical trajectory (if the rails are shifted by approx. 90 degrees, depending on the opening gap), and linear light with arbitrary planes of polarization becomes possible.

2.1.3. Energy Selection

An undulator has the ability to select the photon energies of its preferred emission. This is done by changing the amplitude of oscillation of the electrons,

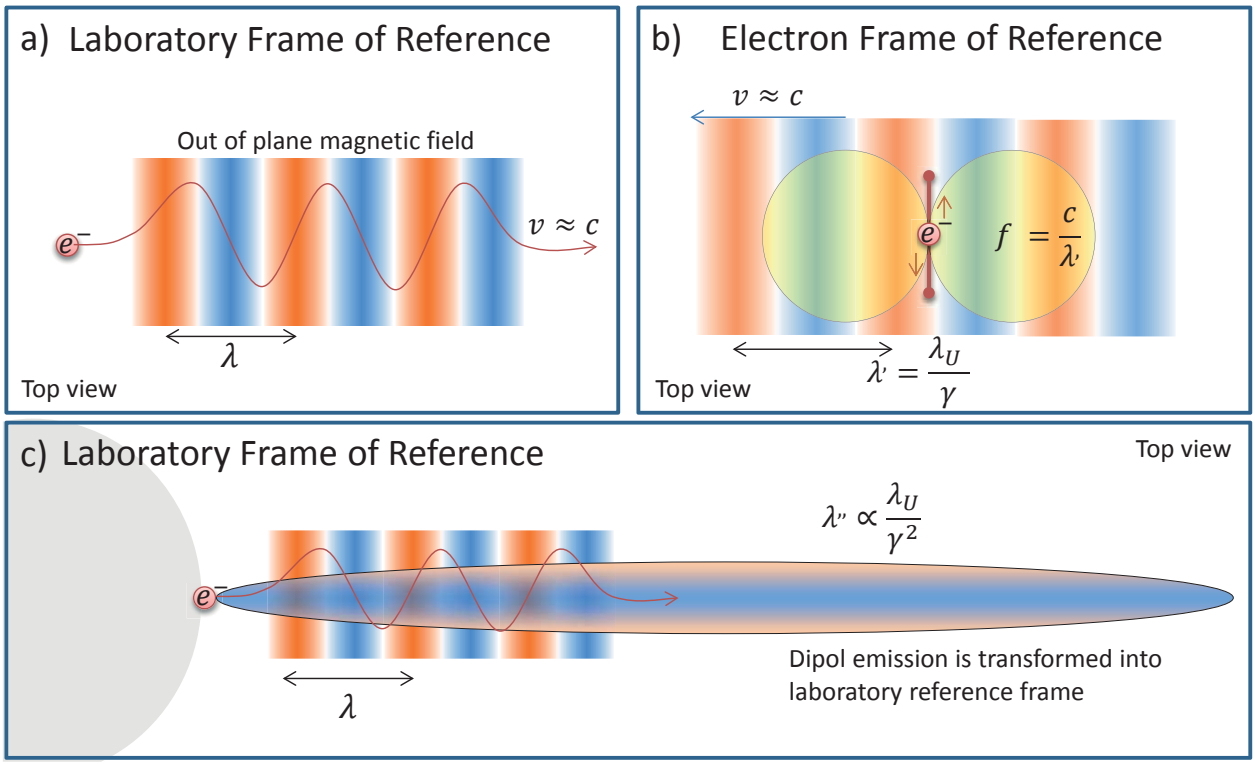

Figure 2.3.: Illustration of the undulator principle. A) shows an electron, from the outside perspective, undulating in the magnetic field of an undulator. B) shows the same from the reference frame of the average electron speed, where the undulator period is compressed due to its relativistic motion. In this reference frame, the electron acts as a dipole emitter with a wavelength given by λ_U/γ. C) shows this radiation from the external reference frame. Its emission pattern is warped into a needle-shaped beam with the wavelength being blue shifted due to it being emitted by an electron moving at relativistic speeds.

which reduces their mean forward velocity. Therefore, γ has to be modified to take this into account, which is done by the dimensionless parameter K [5]:

$$K = \frac{eB_0\lambda_U}{2\pi mc} = 0.934\,\lambda_U[\mathrm{cm}]B_0[\mathrm{T}], \tag{2.4}$$

which scales with the magnetic field B_0 and the undulator period λ_U. The resulting emission wavelength is:

$$\lambda_1 = \frac{\left(1+\frac{K^2}{2}\right)}{2\gamma^2}\cdot\lambda_U \tag{2.5}$$

Large deflection parameters cause a decrease of the average speed of the electrons in direction of the beam axis, which increases the emitted wavelength. This means that counter-intuitively, a *stronger* magnetic field is needed to create photons of *lower* energy when using the same undulator period.

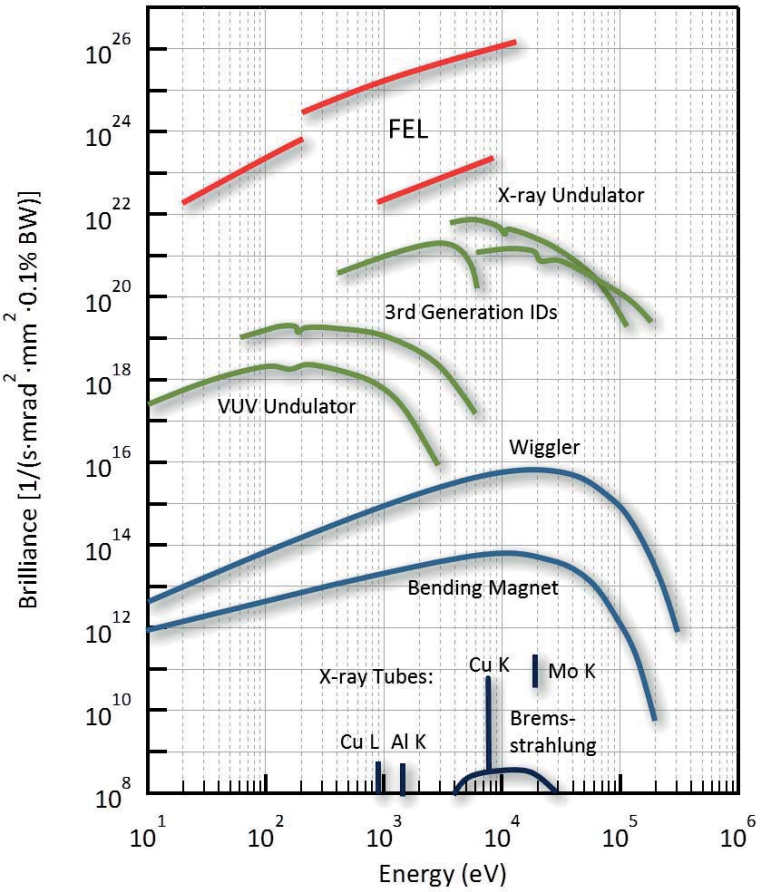

Figure 2.4: Comparison of the brilliance of different X-ray sources. Notably are the extreme jumps between X-ray tubes, bending magnets, undulators and free electron lasers (FEL), each at least improving by 3 orders of magnitude on the other. Adapted from [4].

The deflection parameter, and thus the energy of the emitted photons, can be modified by changing the gap between the magnetic rails shown in Fig. 2.2. On the low end, the energy limit is given by how far the undulator can close, a geometric constraint due to the need of having a vacuum line between the rails of the undulator. The upper limit is given for an undeflected electron, which can be approached by extreme widening of the gap accompanied by a drastic drop in beam intensity.

2.1.4. Undulator Harmonics and Emission Profile

A real undulator does not emit a singular photon energy, but a spectrum of higher harmonics of a base frequency as given by Eq. 2.5. Odd harmonics of the base energy are caused by the transverse oscillations of the electrons becoming anharmonic, whereas even harmonics are caused by longitudinal oscillations and do not emit directly on-axis [6].

This allows access to higher photon energies by using the 3^{rd}, 5^{th} or higher harmonic of the base frequency. An example of an emission spectrum can be found later in Fig. 6.4, where also odd harmonics are visible, as a real beamline also accepts slightly off-axis light.

If we compare the light emission of an undulator with the one of a bending magnet, not only does the repeated structure of an undulator shift the emitted power into narrow energy lines, but also concentrates them into a more narrow cone, with an opening angle as given by [5]:

$$\sigma \cong \frac{1}{\gamma}\sqrt{\frac{1+K^2/2}{2Nn}} \tag{2.6}$$

where N is the number of periods of the Undulator, K the deflection parameter and n the undulator harmonic. As K is a small number, we see that the emission angle is reduced by a factor of $\sqrt{N \cdot n}$ compared to bending magnets.

The combination of tighter emission cone and the fact that the spectrum is compressed into narrow, tuneable lines gives undulators orders of magnitude more brightness compared to bending magnets. Together with the ability to freely select the polarization, this makes them perfect as light sources for (magnetic) X-ray microscopy.

2.2. Time Structure

In a synchrotron storage ring, the electrons end up "bunched" in evenly spaced "buckets". The distance between them is in the case of the ALS, CLS, SLS and Bessy II 60 cm, which corresponds to a bucket frequency:

$$f_{ring} = \frac{c}{60\text{ cm}} \approx 499.654\text{ MHz} \tag{2.7}$$

In order to be able to have this equal spacing, the circumference of these storage rings itself is selected as a multiple of 60 cm.

In the case of Bessy II, this yields 400 buckets, while the slightly smaller ALS has 328. As the circumference of the ring has to be exactly a multiple of the bucket spacing, and is also depending on parameters like temperature or the exact steering of the beam orbit in the ring, the exact bucket frequency in practice differs from the value given in Eq. 2.7. Deviations of up to 50 kHz have been measured at the Maxymus beamline at Bessy II. Therefore, active and continuous synchronization of the timebase of dynamic experiments with the ring frequency is required.

The length of the electron bunch inside those buckets is in the order of 25 to 100 ps, depending on the synchrotron as well as the beam current. At Bessy II, a typical bunch length in normal operation is around 35 ps [7]. In addition, there also exists a special operation mode called "Low-Alpha", in

which bunches are compressed further in length, at the cost of them being spatially wider. In this mode, beam currents are lower (10 to 100 mA) and bunch lengths are as short as a few picoseconds [8].

Filling Pattern

The distribution of the current into the different buckets is called the *Filling Pattern* of the synchrotron. The default operation mode of the synchrotrons relevant to this work is called "Multi Bunch mode". Here, most buckets are filled with an average amount of current, except the camshaft bucket, which contains a much higher current than the rest (factor 5 or more), and the gap, a number of unfilled buckets around the camshaft.

In the absence of an attractive potential from the electron beam, ions can disperse during this time. This increases the lifetime of electrons in the storage rings, as scattering between electrons and ions is reduced. The unfilled buckets in the gap allow the ions to disperse and ensure a better beam stability as well as a lower decay rate. A closer look at the details of the filling patter and time structure can be found in Chap. 7.1.3 as well as in Fig. 8.17.

The combination of gap and camshaft is used for certain types of less sophisticated time resolved experiments, where the separation of the camshaft from the rest of the filled buckets by the gap allows gating of slow detectors.

For these experiments a special filling pattern called "Single Bunch" exists, where only one bucket is filled with a high current. For time resolved STXM as covered in this work, this mode is completely unsuitable. At Bessy II, such light is available for several weeks a year.

3. Interactions Between X-Rays and Matter

3.1. Absorption of Soft X-Rays

The attenuation of electromagnetic waves through matter is given by Lambert-Beer's law, where the intensity I inside a medium drops exponentially as a function of the penetration depth x:

$$\frac{I(E)}{I_0(E)} = e^{-\mu(E)\cdot x}, \tag{3.1}$$

with μ being the photon energy E dependent absorption coefficient. For soft X-rays, the absorption is dominated by the photoeffect, with other contributions of elastic and inelastic scattering orders of magnitude lower [9] and thus negligible.

In a heterogeneous material the absorption coefficient can therefore be expressed as the sum of the products of the atomic scattering cross section σ and the atomic density $\rho[\mathrm{cm}^3]$ for each material in the traversed volume:

$$\mu(E) = \sum_n (\sigma_n(E)\cdot\rho_n) \tag{3.2}$$

Penetration depths vary in a wide range depending on photon energies, from many cm for hard X-rays in most materials to the sub-µm range for soft X-rays below 1 keV.

When a photon is absorbed via the photoeffect, a photoelectron is ejected from its initial bound state. Its kinetic energy is the photon energy minus its original binding energy.

Increasing the photon energy allows the excitation of more tightly bound electrons in the target material, which causes two different behaviors for the energy dependence of absorption. Regions with a steady drop of the absorption cross section roughly proportional to E^{-3}, and regions where the cross section suddenly increases with photon energy.

The latter regions are the so called *absorption edges* and are located whenever the photon energy of the absorbed photon is getting high enough to be able to eject electrons from another (deeper, more tighter bound) shell of the target atoms. Both kinds of behavior are visible in Fig. 3.1 in the example of nickel.